Residue 259 in Protein-Tyrosine Phosphatase PTP1B and PTPα Determines the Flexibility of Glutamine 262†

Günther H. Peters,*,‡ Lars F. Iversen,|| Henrik S. Andersen,⊥ Niels Peter H. Møller,# and Ole H. Olsen*,§

Department of Chemistry, MEMPHYS - Center for Biomembrane Physics, Technical University of Denmark, DK-2800 Lyngby, Denmark, Protein Chemistry, Novo Nordisk, DK-2880 Bagsvaerd, Denmark, Signal Transduction, Novo Nordisk, DK-2880 Bagsvaerd, Denmark, Med Chem Research II, Novo Nordisk Park, DK-2760 Måløv, Denmark, and Haemostasis Biochemistry, Novo Nordisk Park, DK-2760 Måløv, Denmark

Received January 15, 2004; Revised Manuscript Received April 6, 2004

ABSTRACT: To study the flexibility of the substrate-binding site and in particular of Gln262, we have performed adiabatic conformational search and molecular dynamics simulations on the crystal structure of the catalytic domain of wild-type protein-tyrosine phosphatase (PTP) 1B, a mutant $PTP1B_{R47V,D48N,M258C,G259Q}$, and a model of the catalytically active form of PTPα. For each molecule two cases were modeled: the Michaelis−Menten complex with the substrate analogue *p*-nitrophenyl phosphate (*p*-PNPP) bound to the active site and the cysteine-phosphor complex, each corresponding to the first and second step of the phosphate hydrolysis. Analyses of the trajectories revealed that in the cysteine-phosphor complex of PTP1B, Gln262 oscillates freely between the bound phosphate group and Gly259 frequently forming, as observed in the crystal structure, a hydrogen bond with the backbone oxygen of Gly259. In contrast, the movement of Gln262 is restricted in PTPα and the mutant due to interactions with Gln259 reducing the frequency of the oscillation of Gln262 and thereby delaying the positioning of this residue for the second step in the catalysis, as reflected experimentally by a reduction in k_{cat}. Additionally, in the simulation with the Michaelis−Menten complexes, we found that a glutamine in position 259 induces steric hindrance by pushing the Gln262 side chain further toward the substrate and thereby negatively affecting K_m as indicated by kinetic studies. Detailed analysis of the water structure around Gln262 and the active site Cys215 reveals that the probability of finding a water molecule correctly positioned for catalysis is much larger in PTP1B than in $PTP1B_{R47V,D48N,M258C,G259Q}$ and PTPα, in accordance with experiments.

The phosphorylation/dephosphorylation of tyrosine residues in proteins is one of several key molecular mechanisms by which living organisms regulate cell growth, proliferation, and differentiation (*1*−*2*). The phosphorylation state of proteins is remarkably dynamic, which enable cells to respond rapidly to discrete changes in environmental conditions (*3*). This dynamic behavior is governed by the opposing actions of protein-tyrosine kinases and protein-tyrosine phosphatases (PTPs),[1] which are integrated within an elaborate signal-transducing network, which converts external environmental stimuli to internal cellular action(s). The defective or inappropriate operation of this network is at the root of a variety of diseases in humans and animals (*4*−*7*). Consequently, the characterization of the individual components and the delineation of this regulatory network have emerged as one of the most active fields in biological research.

The critical roles played by phosphatases in pathological events indicate that the signaling enzymes are suitable targets for pharmacological intervention and that this may be achievable in a selective manner (*8*−*12*). Among the protein-tyrosine phosphatases, PTP1B has recently received much attention due to its role as a negative regulator of insulin signaling (*13*−*16*). Clearly, a selective control of the biological function of PTP1B is a challenging task, and an inhibitor must not only efficiently bind to the specific target enzyme but also do so without impeding the catalytic behavior of closely related enzymes. It is generally believed that the activity of PTPs is dependent on specific substrates containing the requisite structural recognition sites or on confinement of individual PTPs and protein-tyrosine kinases to specific cellular microenvironments (*17, 18*).

PTPs are characterized by having a common active site sequence, the (H/V)CX_5R(S/T) motif (X denotes a nonconserved amino acid residue) (*19*−*21*). This conserved motif defines the binding site for the phosphate moiety of the tyrosyl phosphate substrate and contains a negatively charged, nucleophilic cysteinyl residue (Cys215), as well as a conserved arginine residue (Arg221) (*19, 22*−*24*). The

† Financial support from the Danish National Research Foundation via a grant to the MEMPHYS−Center for Biomembrane Physics (GHP) is aknowledged.

* To whom correspondence should be addressed: ghp@kemi.dtu.dk (G.H.P.) or oho@novonordisk.com (O.H.O.).

‡ Technical University of Denmark.

|| Protein Chemistry, Novo Nordisk.

⊥ Med Chem Research II, Novo Nordisk Park.

Signal Transduction, Novo Nordisk.

§ Haemostasis Biochemistry, Novo Nordisk Park.

[1] Abbreviations: ABNR, adopted basis Newton Raphson; MD, molecular dynamics; PDB, Protein Data Bank; PTP, protein-tyrosine phosphatase; *p*-NPP, *p*-nitrophenyl phosphate; SD, steepest descents.

10.1021/bi0498757 CCC: $27.50
Published on Web 06/10/2004

arginine residue is important in coordinating the phosphate group of the substrate (*25*), and it contributes to stabilizing the negative charge of Cys215 (*19*, *22*, *23*, *26*−*28*). Binding of the substrate triggers the movement of a loop (the "WPD loop") toward the phosphate moiety, which causes a tight binding of the tyrosyl phosphate group and brings the catalytically active aspartate (Asp181) (general acid/base) in position for the catalytic reaction. Cys215 attacks the phosphorus atom in the substrate resulting in the formation of a covalent thiophosphate enzyme intermediate. In the second step, Gln262 coordinates a water molecule that destabilizes the transition state yielding inorganic phosphate (*21*, *22*).

We have previously performed a detailed structural analysis of the variability and conservation of amino acid residues in the vicinity of the active site to identify areas in PTPs that could determine the substrate specificity (*29*). On the basis of Cα regiovariation analyses and primary sequence alignments, we have identified regions in the binding cleft that might confer substrate specificity among PTPs. Among those, residues 47, 48, 258, and 259 (PTP1B numbering) are of particular interest (*29*), since these are involved in substrate specificity and are potential targets for inhibitor design. Position 48 is occupied by an aspartate residue in PTP1B, and selectivity toward substrates or potential inhibitors is governed by electrostatic interactions (i.e., salt bridge formation) (*30*). On the other hand, the selectivity impaired by residues 258 and 259 might be due to steric hindrance. In PTP1B, residue 259 is a glycine, and we hypothesized that the lack of a side chain would allow easy access to the active site, whereas bulky residues in this position in other PTPs might cause steric hindrance. Thus, Gly259 and Cys258 in PTP1B form the bottom of an open cleft, a gateway, which leads to the active site (*31*, *32*). Indeed, using a mutational approach we demonstrated that replacing Gly259 in PTP1B with a glutamine caused steric hindrance and concomitant restricted substrate recognition. In contrast, by substituting Gln259 for a glycine in PTPα, we obtained an enzyme with broad substrate recognition capacity, that is, an enzyme similar to PTP1B (*31*). Recently it was reported that PTP1B has the capacity to bind and dephosphorylate substrates with two adjacent phosphotyrosine residues, which is observed in the insulin receptor tyrosine kinase activation loop (*32*). This is achieved through simultaneous binding of the phosphotyrosine residues to the active site and a second aryl phosphate binding site, which was previously identified by Zhang and co-workers (*33*). Hence, residue 259 may be translated directly into functional consequences relating to insulin signaling.

Our previously conducted studies also point to a more complex picture regarding the involvement of residue 259 in substrate recognition and hydrolysis (*31*). The results indicated that bulky residues in position 259, in addition to the described steric hindrance, indirectly might influence the catalytic activity of PTPs by an interference with the conformational freedom of residue 262. Therefore, to further evaluate the influence of residue 259 on Gln262, we have performed adiabatic conformational search and molecular dynamics (MD) simulations with the catalytic domain crystal structures of PTP1B, a mutant of PTP1B in which a defined set of four residues have been introduced as a model for PTPα, and a model of the active form of PTPα. The latter

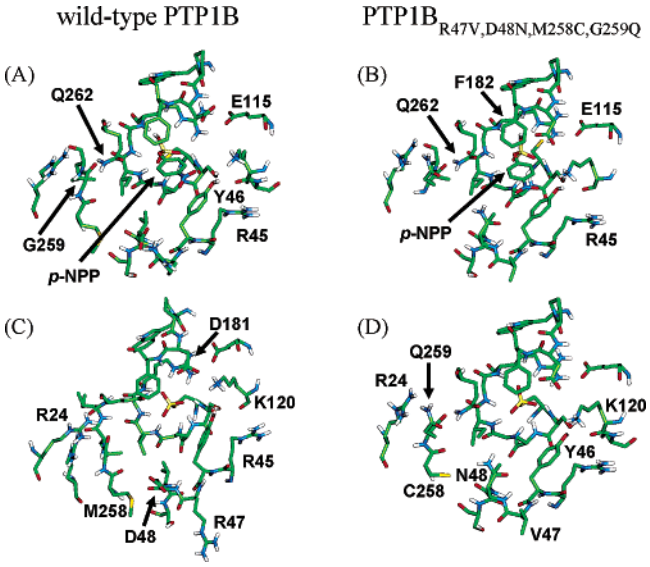

FIGURE 1: Active site regions of PTP1B and the mutant PTP1B$_{R47V,D48N,M258C,G259Q}$ are shown in liquorice representation and colored according to atom type. Panels A and B display PTP1B and PTP1B$_{R47V,D48N,M258C,G259Q}$, respectively, in complex with *p*-NPP (Michaelis−Menten complex). Panels C and D show the cysteinyl-phosphate intermediate complex of PTP1B and PTP1B$_{R47V,D48N,M258C,G259Q}$, respectively.

two enzymes are representative for PTPs with bulky residues in position 259. For each molecule two cases are modeled: the Michaelis−Menten complex with the substrate analogue *p*-nitrophenyl phosphate (*p*-NPP) bound to the active site and the cysteine-phosphor complex. The simulations are analyzed to elucidate the conformational space explored by Gln262 along the trajectories and to identify key interactions between Gln262 and residues residing in the vicinity of Gln262 that might affect the dynamics of Gln262.

MATERIALS AND METHODS

The crystal structures of (i) PTP1B bound with phosphate (cysteinyl-phosphate intermediate) resolved to 2.5 Å (*34*), (ii) PTP1B complexed with a hexapeptide resolved to 2.6 Å (*35*), and (iii) PTPα resolved to 2.25 Å (*36*) were obtained from the Protein Data Bank at Brookhaven (*37*; PDB entry codes 1a5y, 1ptu, and 1yfo, respectively). The structure of the mutant of PTP1B (PTP1B$_{R47V,D48N,M258C,G259Q}$) resolved to 2.13 Å was obtained from Novo Nordisk A/S (*31*; PDB entry code 1gfy). In the crystal structure of PTPα, the WPD loop is in the open, noncatalytic conformation. To make a model of the catalytically active enzyme, the WPD loop has been modeled in the so-called closed conformation using PTP1B as a template. This PTPα structure will be referred to as the model structure of PTPα throughout. In total, six models were examined: the enzyme/*p*-NPP complex and the cysteinyl-phosphate intermediate for wild-type PTP1B, PTP1B$_{R47V,D48N,M258C,G259Q}$, and PTPα. We used the PTP1B structure complexed with the hexapeptide as a template to place the substrate *p*-NPP into the active site of PTP1B, PTP1B$_{R47V,D48N,M258C,G259Q}$, and PTPα. In Figure 1, the active site regions of PTP1B and the mutant of PTP1B of the Michaelis−Menten and cysteine-phosphor complex are depicted. The total charge of *p*-NPP was set to −1 with the following partial charges: N = +0.8, O (in NO_2) = −0.4, C_γ = 0.0, $C_{\delta 1}$ = 0.0, $C_{\epsilon 1}$ = 0.0, $C_{\delta 2}$ = 0.0, $C_{\epsilon 2}$ = 0.0, C_ζ =

0.0, P = +0.90, OH = −0.46, OC1 = −0.62, OC2 = −0.62, OT = −0.60, HT = +0.40. The charges are in accordance with the charges in the CHARMm22 force field. The charges for the phenyl phosphate correspond to the charges in the side chain of phosphorylated tyrosine (residue id in CHARMm22: PTYR).

Adiabatic Mapping. To characterize the configurational space explored by Gln262 in the three enzymes under investigation, the adiabatic energy was evaluated for a discrete set of side chain conformations obtained by systematically constraining the χ_i angles (from 180° to −180° in steps of 30°) of Gln262 in the wild-type PTP1B and Gln259/Gln262 in the mutant structure of PTP1B and in the model structure of PTPα. The CHARMm22 molecular modeling package (*38*) with polar hydrogens was applied. The procedure was as follows: The side chain conformation was established and constrained using a dihedral potential with a barrier height of 1000 kcal/mol (the so-called *cons DIHE* facility in CHARMm22 was applied). Apart from the side chain(s) atoms in question the remaining enzyme atoms were fixed. An energy minimization was performed using 25 steps of steepest descents (SD) followed by 25 steps of adopted basis Newton Raphson (ABNR). The electrostatics was modeled using a distance dielectric model, that is, the energy is proportional to $10/r^2$ where r is the distance between interacting charged atoms and 10 is an appropriate scaling factor. If either the van der Waals or the electrostatic interaction energy was positive, the side chain configuration was discarded. However, if the interaction energies were negative, another energy minimization round was performed, where atoms within 5 Å from the side chain(s) in question were free to move. The minimization procedure consisted of 75 steps of SD and 75 steps of ABNR. Energies were monitored and the corresponding conformations were saved.

Molecular Dynamics Simulations. For the MD simulations, the structures were solvated with an equilibrated TIP3 water sphere (*39*). All water molecules within 2.4 Å of any non-hydrogen protein atom were removed. The total system consisted of approximately 15 300 atoms. Atoms located within 20 Å from the active site (Cys215) were allowed to move freely, which accounted for approximately 10 900 atoms. A so-called extended wall region (*40*) was applied from 20 to 24 Å counting for approximately 1900 atoms. The motions of the atoms in this region were restrained to their initial positions by a harmonic potential with a force constant of 500 kcal/(mol Å^2). All atoms in the remaining part of the molecule were fixed at their original positions. The different regions are displayed in Figure 2A for the cysteinyl-phosphate intermediate of PTP1B (*34*) (top view). The color scheme is as follows: blue denotes that atoms can freely move; red denotes that atoms are constrained by a harmonic potential; green denotes that atoms are fixed. Figure 2B shows the solvated structure where, for clarity, only the oxygens of the water molecules are displayed in red and in van der Waals modus (top view). In Figure 2C, we have only included water molecules that are free to move in the simulations (top view). Figure 2D is a side view of Figure 2C. Our choice of the boundary was based on the following observations: (i) comparison of the structures of PTP1B in complex with different ligands, which are available from the Protein Data Bank, revealed that the structural changes upon binding of the different ligands are localized close to the active site; (ii) essential dynamics analysis of a 1-ns trajectory obtained from MD simulations of PTP1B in complex with a natural substrate indicate that the predominant internal motions in PTP1B occur mainly in the binding pocket (*41*, *42*). For all simulations, the MD program CHARMm (*38*) was used with the CHARMm22 polar hydrogen parameter set and with the TIP3 water model (*39*). Ten 1-ns simulations were performed for each the Michaelis−Menten complex and the cysteinyl-phosphate intermediate for PTP1B and $PTP1B_{R47V,D48N,M258C,G259Q}$. These simulations were supplemented by three 1-ns simulations on PTPα with substrate in Michaelis−Menten complex or the cysteinyl-phosphate intermediate. The initial starting configurations were generated by using different extents of minimization. The initial system was subjected to 10, 30, 50, 70, 90, 110, 130, 250, 375, or 500 steps of both steepest decent and conjugated gradient energy minimization. After minimization, the models (which were based on X-ray crystallographic structures) involving PTP1B and $PTP1B_{R47V,D48N,M258C,G259Q}$ deviated less than 0.4 Å in rmsd on the Cα atoms from their crystal structure. For the two models (which were homology built) involving PTPα the corresponding rmsd deviation was less than 0.7 Å. The minimization was followed by a 3 ps heating period to the final temperature of 300 K. A time step of 1 fs was employed throughout, and the SHAKE algorithm was applied for all hydrogen atoms. The nonbonded forces were shifted and truncated at 10 Å, and the atom pair list was updated every 0.01 ps. Configurations for later analyses were saved every 500 steps.

RESULTS AND DISCUSSION

Protein-tyrosine phosphatases (PTPs) utilize a two-step reaction to cleave phosphate from tyrosine-phosphorylated residues. The key components of catalytic machinery consist of the active site Cys215, the general acid/base Asp181, and the water-coordinating residue Gln262 (*21*). The first step is initiated by a nucleophilic attack of the active site cysteine on the phosphorus atom of the bound substrate. As the ester bond is cleaved, Asp181 donates its proton to the leaving group oxygen. This substitution reaction leaves the phosphate group covalently attached to the nucleophile via a thioester linkage.

In the second step of the reaction, which involves hydrolysis of the phosphoenzyme, a water molecule acts as the nucleophile. Asp181 activates the water by abstracting one of its hydrogens. This reaction requires that the hydrolytic water molecule is perfectly positioned in the active site for efficient hydrolysis. It has been shown experimentally that Gln262 in PTP1B coordinates this water molecule (*34*, *43*). Thus, mutation of Gln262 to an alanine results in dramatic reduction of both k_{cat}/K_m and k_{cat} for the hydrolysis of the EGF-R derived peptide, suggesting that Gln262 plays a role both in the E-P formation and the E-P hydrolysis step (*11*, *21*, *44*). In an elegant study, the prolongation of the lifetime of the cysteinyl-phosphate intermediate in the $PTP1B_{Q262A}$ mutant was visualized by X-ray crystallography (*34*, *45*). Inspection of all PTP crystal structures available at the Protein Data Bank reveals that Gln262 points outward from the active site and forms a hydrogen bond with the backbone oxygen of Gly259 (Gln262(Hε)−Gly259(O) hydrogen bond). This position of Gln262 allows efficient

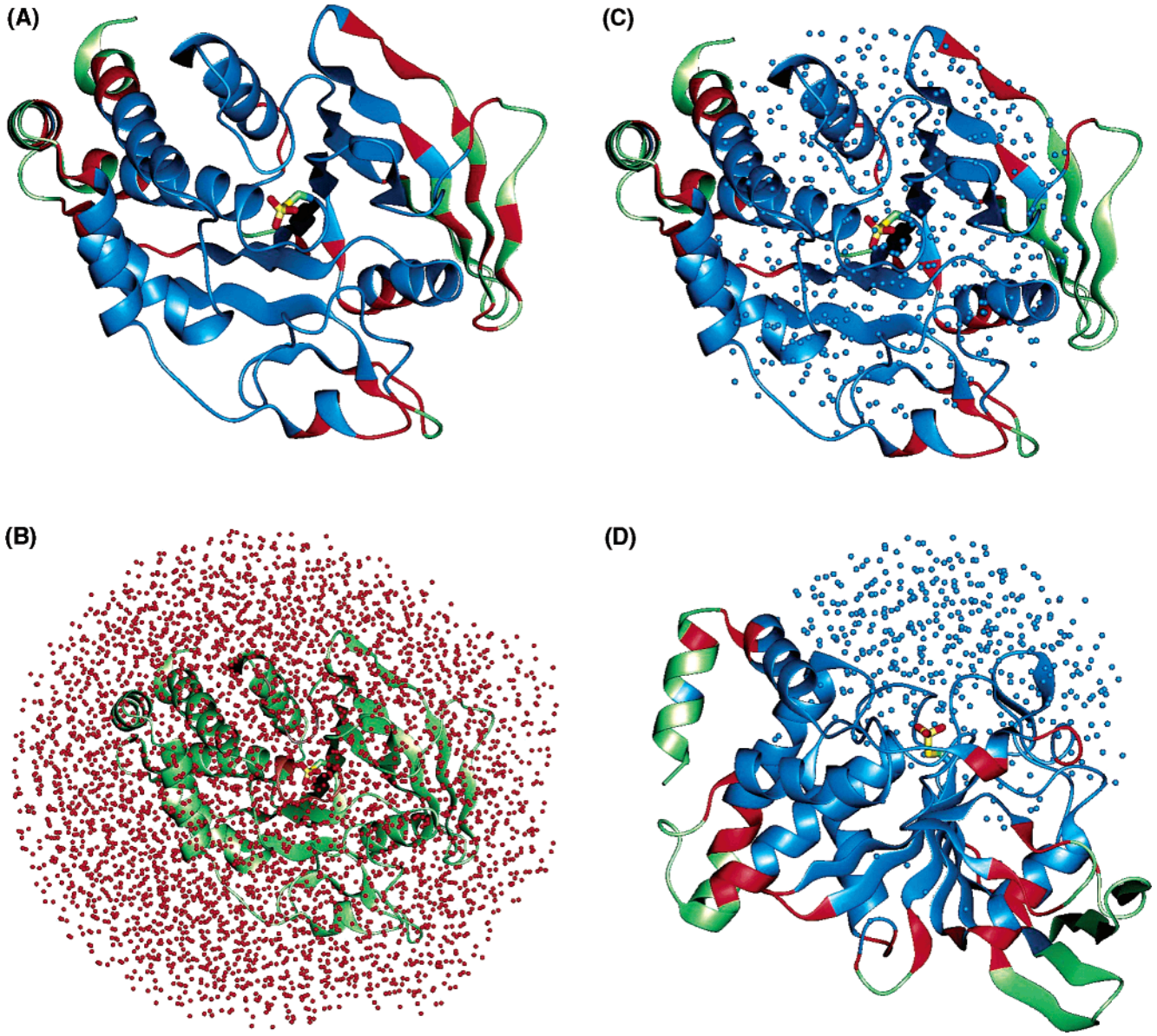

FIGURE 2: Secondary structure of PTP1B with covalently bound phosphate (cysteinyl-phosphate intermediate; *34*). The structure is oriented such that the view is into the active site pocket with the phosphate group bound to the active site cysteine (Cys215) in the center. Panel A shows the region included in the simulations; atoms located within a distance of 20 Å from Cys215 are free to move, and this region is colored blue. Harmonic constraints were applied to atoms in the range from 20 to 24 Å from the active site (colored red). Atoms beyond 24 Å were fixed (colored green). Panel B shows the solvated structure. For clarity, only the oxygens of the water molecules are shown in the van der Waals representation and are colored red. Panel C shows the top view of the solvated structure where only the water molecules that are located within 20 Å from the Cys215 (colored blue) are shown. Panel D shows the side view of the solvated structure where only the water molecules that are located within 20 Å from the Cys215 (colored blue) are shown.

binding of substrates (and active-site-directed inhibitors), and the close proximity to the phenyl ring of the substrate makes it part of the pTyr binding pocket. In the second step of the reaction, however, the Gln262 side chain has to move into the pocket to coordinate the hydrolytic water molecule, thus requiring Gln262 to have a certain flexibility to efficiently participate in the hydrolysis. Any impairment of the side chain mobility should have influence on the kinetics of the hydrolysis, thereby altering the Michaelis−Menten constants K_m and k_{cat}. Indeed, we have shown experimentally that for the substrate *p*-NPP, K_m increases and k_{cat} decreases when Gly259 is mutated to the bulky residue glutamine (*31*, *46*).

We have previously shown experimentally that residues 258 and 259 in PTP1B and TC-PTP form the bottom of a "gateway" that allows easy access of pTyr substrates to the active site of these PTPs. In PTP1B, TC-PTP, and a few other PTPs, residue 259 is a glycine, whereas in most PTPs residues with bulky side chains occupy this position. As a result, the 258/259 gateway is less accessible, thereby leading to less efficient substrate binding and catalysis (*31*, *46*, *47*).

To further define the role of bulky 262-residues in the catalysis and to elucidate their mobility and interactions with neighboring residues, we here compare PTP1B, a four-point mutant of PTP1B ($PTP1B_{R47V,D48N,M258C,G259Q}$), and PTPα in adiabatic conformational mapping experiments, as well as molecular dynamics simulations. PTP1B and PTPα are biologically important enzymes in signal transduction (*48*−*52*). However, the catalytically active form of PTPα has not been resolved by X-ray crystallography. Therefore we have built a model structure of PTPα using the inactive form of

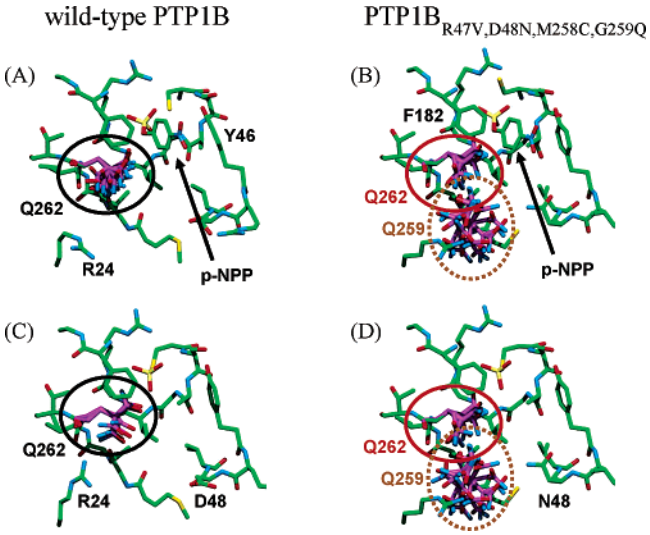

FIGURE 3: Graphical presentation of the results of the adiabatic conformational search. For clarity, only the active site region is displayed and shown in liquorice representation. The carbon atoms of the side chain Gln259 and Gln262, the conformations of which were systematically changed during the search, are colored purple. Oxygens and nitrogens are colored red and blue, respectively. Only conformations yielding negative interaction energies between Gln259 and Gln262 are selected and shown. Panels A and B display the side chain conformations of Gln262 in PTP1B and of Gln259 and Gln262 in $PTP1B_{R47V,D48N,M258C,G259Q}$, respectively, when in complex with *p*-NPP (Michaelis−Menten complex). Panels C and D show the side chain conformations of the corresponding residues in the cysteinyl-phosphate intermediate complex of PTP1B and $PTP1B_{R47V,D48N,M258C,G259Q}$, respectively.

PTPα and PTP1B as a template. Since our PTPα structure is a model and in this respect a "low-resolution" structure, we also have included the high-resolution structure of the mutant $PTP1B_{R47V,D48N,M258C,G259Q}$, which despite the fact that it only differs in four positions compared to PTP1B, behaves kinetically similarly to PTPα (*31*). Because the modeling experiments rely on high-resolution structural information, we have more intensively studied PTP1B and $PTP1B_{R47V,D48N,M258C,G259Q}$ than PTPα. By including the $PTP1B_{R47V,D48N,M258C,G259Q}$ mutant in our analysis, we can directly evaluate the role of the gatekeeper, that is, Gln259, and simultaneously evaluate the model of PTPα.

In the following, we will consider distances only, since they correlate with the interaction energies between the atoms; that is, a short distance implied a negative (favorable) interaction energy. We will first discuss the results of the adiabatic conformational mapping experiments, followed by a presentation of the MD simulations.

Conformational Freedom of Gln262/Gln259. To characterize the configurational space explored by Gln262 with and without the presence of Gln259, an adiabatic energy contour map was constructed by successively constraining the $\chi 1$ and $\chi 2$ dihedral angles (from 180° to −180° in steps of 30° resulting in $6 \times 6 \times 6 \times 6 = 1296$ independent conformations). The configurations shown in Figure 3 are selected according to the energy criterion described in the Materials and Methods section. The conformations of Gln262 (and Gln259 in $PTP1B_{R47V,D48N,M258C,G259Q}$) all have negative interaction energies with the protein.

In Figure 3A,B, the results are shown for PTP1B and $PTP1B_{R47V,D48N,M258C,G259Q}$ in complex with *p*-NPP. Gln262 in PTP1B (Figure 3A) is free to move and can adopt a wide spectrum of low energetic conformations allowing easy access of *p*-NPP to the active site cysteine. The major portion of conformations of the Gln262 side chain exhibits no steric clashes to *p*-NPP, since Gln262 can move away from the substrate without paying an energy penalty. Among the low-energy conformations, we also observe a conformation of Gln262 that is close to Gly259 with the possibility of hydrogen bond formation with the backbone oxygen of Gly259. In contrast, the mutant has a reduced number of low-energy conformations of Gln262 due to the presence of a glutamine in position 259 that restricts the conformational space of Gln262 resulting in a reduced access of *p*-NPP to the active site cysteine. Thus *p*-NPP has to overcome an energy barrier to bind to the active site cleft (i.e., the substrate has to push away Gln262) giving rise to the experimentally observed higher K_m value for $PTP1B_{R47V,D48N,M258C,G259Q}$ than for the wild-type PTP1B (*31*). Clearly, Gln262 takes a conformation located between the phosphate group of *p*-NPP and Gln259. Steric hindrance prevents Gln262 from forming a hydrogen bond with the backbone oxygen of Gln259. For the cysteinyl-phosphate intermediate complex (Figure 3C,D), we observe that Gln262 can freely move in PTP1B. However, two orientations dominate. One is in a position that would allow coordination of the hydrolytic water molecule that participates in the second step of hydrolysis. In the other orientation, the side chain amide generates a hydrogen bond to the main chain carbonyl of Gly259. Hence in this simple picture, the conformation that promotes the interaction to the catalytic water molecule is highly populated. The presence of explicit solvent may increase this population because of a possible favorable interaction to a solvent molecule.

In contrast to the wild-type enzyme and similar to the situation in PTPα (data not shown), the conformation of Gln262 in $PTP1B_{R47V,D48N,M258C,G259Q}$ is influenced by the interaction to the side chain of Gln259. Therefore a large portion of the side chain orientations point away from the phosphate moiety and thereby lack the possibility of positioning the catalytic water molecule, consistent with the experimental observation that k_{cat} is decreased for $PTP1B_{R47V,D48N,M258C,G259Q}$.

Simulations: PTP1B Complexed with p-NPP or with Covalently Bound PO_4. The results presented in the previous section, however, only provide a qualitative description of the conformational freedom of Gln262, neglecting the flexibility of the neighboring residues and the presence of explicit solvent molecules. Hence, to overcome these shortcomings, we have in the following performed MD simulations that allow the free motion of side chains in the binding pocket in the presence of explicit solvent.

The catalytic reaction requires that several residues act in a correlated fashion. As discussed above, the movement of the WPD loop occurring after binding of the substrate is followed by the movement of the side chain of Gln262. Gln262 swings into the binding pocket to coordinate a water molecule that takes part in the second step of the hydrolysis. Any impairment of the movement of Gln262 in the Michaelis−Menten complex or in the cysteinyl-phosphate intermediate could affect the catalytic efficiency and explain the experimentally observed differences in the kinetic constants (K_m, k_{cat}) when comparing PTP1B with the mutant $PTP1B_{R47V,D48N,M258C,G259Q}$ or PTPα. PTP1B is one of the most

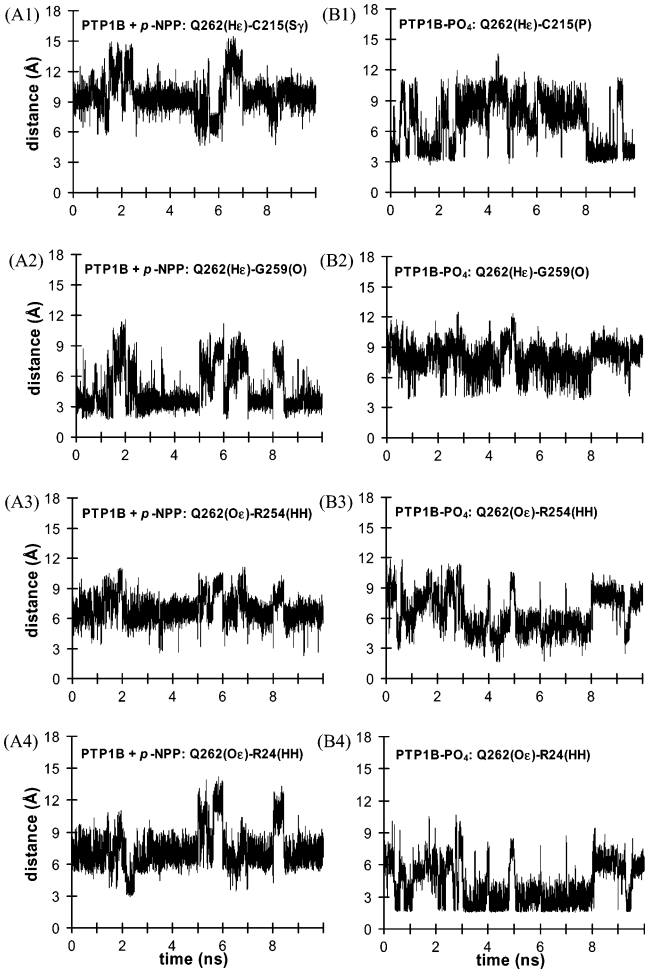

FIGURE 4: The time evolution of distances between selected residues obtained from the 10 1-ns simulations. Distances shown in panels A and B are extracted from the simulations of PTP1B with bound substrate *p*-NPP and with covalently bound phosphate, respectively. The distances monitored in the PTP1B + *p*-NPP simulations are (A1) Q262(Hϵ)−C215(Sγ), (A2) Q262(Hϵ)−G259-(O), (A3) Q262(Oϵ)−R254(HH), and (A4) Q262(Oϵ)−R24(HH). The corresponding distances extracted from the PTP1B−PO_4 simulations are shown on the right and labeled B1−B4.

efficient enzymes in hydrolyzing *p*-NPP or phosphorylated peptides (*47* and references therein), and hence, the movement of Gln262 is likely to be optimal for hydrolysis. We therefore studied first PTP1B and used the results as a reference point when studying $PTP1B_{R47V,D48N,M258C,G259Q}$ and PTPα. To extract information regarding the mobility of Gln262 and its neighboring residues (and thereby elucidating possible key interactions between Gln262 and surrounding residues), we have performed MD simulations on PTP1B complexed with *p*-NPP or covalently bound phosphate. The time evolution of distances between selected residues obtained from the 10 1-ns simulations are shown in Figure 4 for the PTP1B-*p*-NPP complex (left panels, A1−A4) and the cysteinyl-phosphate intermediate (right panels, B1−B4). The distances shown correspond to Gln262−Cys215 (Figure 4A1,B1), Gln262−Gly259 (Figure 4A2,B2), Gln262−Arg254 (Figure 4A3,B3), and Gln262−Arg24 (Figures 4A4,-B4). The time evolution of the distances shown are based on 10 independent 1-ns simulations, and the distances extracted from each simulation have been drawn sequentially. A very interesting picture evolves for the mobility of Gln262. In the Michaelis−Menten complex, Gln262 frequently forms a hydrogen bond with the oxygen backbone of Gly259 (Figure 4A2). Its movement is restricted due to the presence of the substrate molecule *p*-NPP, which prevents the side chain from swinging into the binding pocket (Figure 4A1). The probability that Gln262 interacts with the neighboring residues Arg254 (Figure 4A3) or Arg24 (Figure 4A4) is significantly lower in the Michaelis−Menten complex than in the simulations on the cysteinyl-phosphate intermediate. For the cysteinyl-phosphate intermediate, short distances (i.e., strong interactions) are frequently seen between Gln262 and Arg24 (Figure 4B4). Short distances are also monitored between Gln262 and Arg254 (Figure 4B4), but the frequency of occurrence is significantly lower than that observed for the Gln262−Arg24 distances (Figure 4B3) indicating that this interaction might be of less importance. Our analysis reveals that Gln262 oscillates between Arg24 and Cys215, thereby frequently taking up a position that would allow the coordination of the water molecule that participates in the second step of hydrolysis. The positioning of the water molecule will be addressed in more detail below. In contrast to the simulations on the Michaelis−Menten complex, no short distances (i.e., <3 Å) are monitored in the simulations on the cysteinyl-phosphate intermediate (Figure 4B2) between Gln262 and the carbonyl of Gly259. To further quantify the results, we have calculated the probability distributions as a function of distances and estimated the corresponding standard deviation (Figure 5). Some of the data points in the different distributions have relatively high standard deviations, which, according to Figure 4, is not only due to relatively large fluctuations in the distances but also due to the sampling from independent simulations. In the following, we will only discuss the probability distributions of distances between selected residues to ease the comparison between the simulations on the different enzymes.

Simulations: Mutant of PTP1B Complexed with p-NPP or with Covalently Bound PO_4. The results described above for PTP1B revealed that Gln262, in particular, interacts with Gly259 (backbone oxygen), Arg24, and Arg254. We therefore monitored the interaction patterns from Gln262 and Gln259 in $PTP1B_{R47V,D48N,M258C,G259Q}$ with neighboring residues. The probability distributions of distances between selected residues are shown in Figures 6 and 7. The distributions were calculated from the time evolution of the distances between Gln262−Cys215 (Figure 6A1,B1), Gln262−Gln259 (Figure 6A2,B2), Gln262−Arg254 (Figure 6A3,B3), Gln262−Arg24 (Figure 6A4,B4), Gln259−Arg24 (Figure 7A1,B1), Gln259−Arg254 (Figure 7A2,B2), and Gln259−Gln262 (Figure 7A3,B3), which were extracted from the simulations on the Michaelis−Menten complex (left panels, labeled A) and on the intermediate (right panels, labeled B).

For the simulations on the Michaelis−Menten complex of $PTP1B_{R47V,D48N,M258C,G259Q}$, the probability distributions (i.e., interaction pattern) are qualitatively similar to the ones determined for the wild-type PTP1B (Figures 6A1−A4 vs 5A1−A4). As expected, due to the presence of the gatekeeper Gln259, the only significant difference is that the probability of observing a hydrogen bond distance between Gln262 and the oxygen backbone of Gln259 is lower than that monitored in wild-type PTP1B (see Figures 5A2 and 6A2). This observation is in contrast to the conformational search (i.e., adiabatic energy contour map), where no hydrogen bond distance between Gln262 and the backbone oxygen of

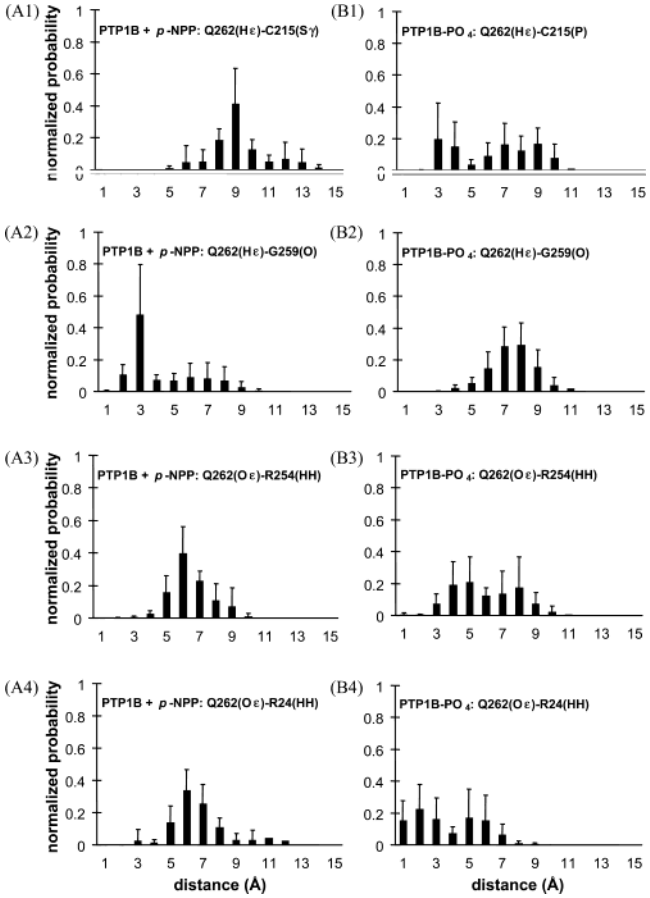

FIGURE 5: Normalized probability functions of distances between selected residues, which are calculated from the time evolution of the distances shown in Figure 4. The bins in the histograms have been defined by taking the integer part of the distances. See Figure caption 4 for more details.

Gln259 was monitored. This underlines the shortcoming of the conformational search, which does not take into account the dynamics (flexibility) of neighboring residues (as included by MD). For the simulations on the cysteinyl-phosphate intermediate, Gln262 shows a different behavior than that in the simulations on the wild-type PTP1B. The probability distribution of distances in the mutant between Gln262 and Cys215 is shifted to larger distances (Figure 5B1 vs 6B1), and additionally the frequency at which Gln262 interacts with Arg254 or Arg24 is reduced (Figure 5B3 vs 6B3), since the bulky residue Gln259 impairs with the interactions of Gln262 with the two arginine residues. This is clearly seen in Figure 7. In the Michaelis−Menten complex, the strongest interactions are found between Gln259 and Arg24, where a high probability is observed at short distances (Figure 7A1). This indicates that the conformational freedom of Gln259 is restricted due to interactions with Arg24. In contrast, the interaction of Gln259 with Arg254 or Gln262 is less pronounced than that with Arg24, which is reflected in a distribution with a maximum at relatively large distances (Arg254; Figure 7A2) or in a broad distribution without a preferable distance (Gln262; Figure 7A3). Noticeably, the behavior of Gln259 in the simulations on the intermediate is reversed; that is, the strongest interactions are now found between Gln259 and Arg254 (Figure 7B2), the distribution of Gln259−Arg24 is shifted to larger distances (Figure 7B1 vs 7A1), and there is a higher probability of encountering interactions between Gln259 and

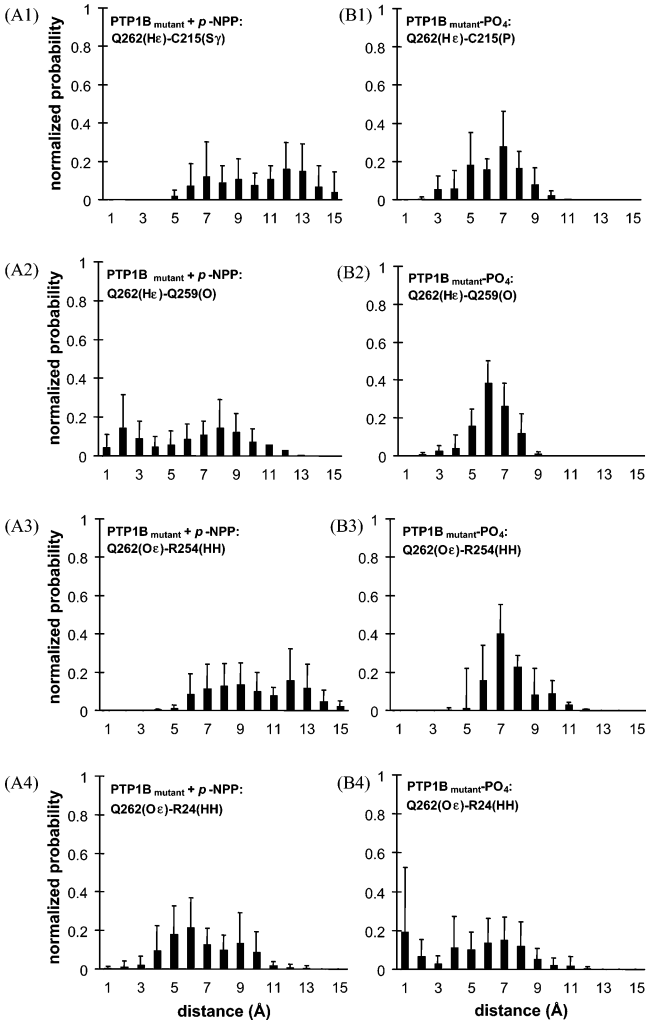

FIGURE 6: Normalized probability functions of distances between selected residues, which are calculated from the time evolution of the distances (data not shown). Distances shown in panels A and B are extracted from the simulations of $PTP1B_{R47V,D48N,M258C,G259Q}$ with bound substrate *p*-NPP and with covalently bound phosphate, respectively. The distances monitored in the $PTP1B_{R47V,D48N,M258C,G259Q}$ + *p*-NPP simulations are (A1) Q262(Hε)−C215(Sγ), (A2) Q262(Hε)−Q259(O), (A3) Q262(Oε)−R254(HH), and (A4) Q262(Oε)−R24(HH). The corresponding distances extracted from the $PTP1B_{R47V,D48N,M258C,G259Q}$−$PO_4$ simulations are shown on the right and labeled B1−B4. See caption for Figure 5 for definition of the histogram.

Gln262 (Figure 7B3 vs 7A3). Clearly, our simulations demonstrate that the mobility of Gln262 is affected by the presence of the bulky side chain Gln259 thereby impairing the coordination of the water molecule that is involved in the second step of the catalysis. For catalysis several events have to act in a concerted fashion. Interference of one of the steps (such as the coordination of a water molecule participating in the second step of the catalysis) will affect other events thereby changing the probability of successful catalysis. This is reflected in the experimentally observed reduced turn over number (i.e., k_{cat}) when wild-type PTP1B and the mutant $PTP1B_{R47V,D48N,M258C,G259Q}$ are compared.

Key Interactions. The simulations on PTP1B and $PTP1B_{R47V,D48N,M258C,G259Q}$ point to the conclusion that the presence of a bulky side chain in position 259 changes the key interactions between the side chain of Gln262 and neighboring side chains in the active site cleft. For PTP1B in the Michaelis−Menten complex, the side chain of Gln262

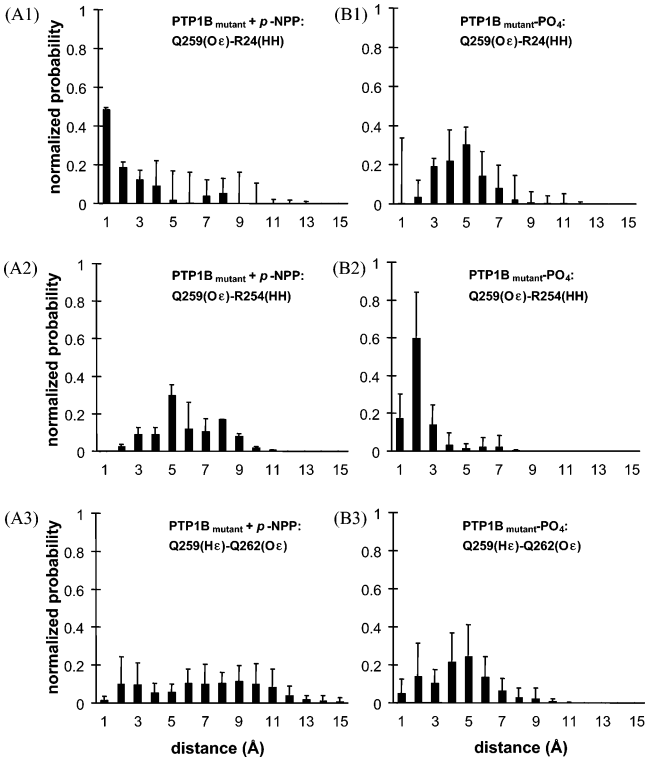

FIGURE 7: Normalized probability functions of distances between selected residues, which are calculated from the time evolution of the distances (data not shown). Distances shown in panels A and B are extracted from the simulations of PTP1B$_{R47V,D48N,M258C,G259Q}$ with bound substrate *p*-NPP and with covalently bound phosphate, respectively. The distances monitored in the PTP1B$_{R47V,D48N,M258C,G259Q}$ + *p*-NPP simulations are (A1) Q259(Oε)−R24(HH), (A2) Q259(Oε)−R254(HH), and (A3) Q259(Hε)−Q262(Oε). The corresponding distances extracted from the PTP1B$_{R47V,D48N,M258C,G259Q}$−PO_4 simulations are shown on the right and labeled B1−B3. See caption for Figure 5 for definition of the histogram.

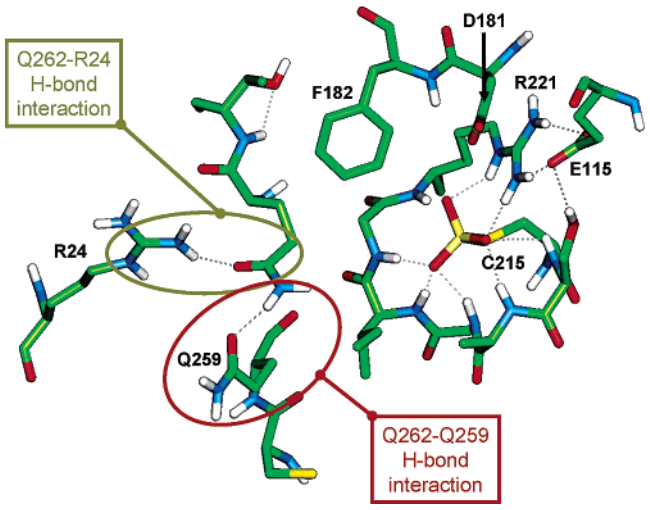

FIGURE 8: Key interactions in the binding pocket of the cysteinyl-phosphate intermediate of PTP1B$_{R47V,D48N,M258C,G259Q}$. Key interactions between glutamine 262 and arginine 24, as well as glutamine 262 and glutamine 259, are indicated. Hydrogen patterns are shown by dashed lines.

interacts strongly with the main chain carbonyl of Gly259, while in the cysteinyl-phosphate intermediate of PTP1B the side chain of Gln262 oscillates between positions close to Cys215 and Arg24 (and to a less extent to Arg254). In the Michaelis−Menten complex of PTP1B$_{R47V,D48N,M258C,G259Q}$, Gln262 primarily binds to Arg24 (and less often to the side chain and main chain carbonyl of Gln259). Interestingly, in this complex the orientation of Gln259 is stabilized by an interaction to Arg24. In the cysteinyl-phosphate intermediate for the mutant the interaction of Gln262 with Cys215 is less frequent compared to the situation for PTP1B. Of notice, Gln262 takes up a tight interaction to Arg24 and at the same time maintains the interaction to the side chain of Gln259. In Figure 8, a snapshot taken from an MD trajectory of this interaction is displayed.

Simulations: PTPα Complexed with p-NPP or with covalently bound PO4. The simulation results for the cysteinyl-phosphate intermediate of PTP1B and the mutant PTP1B$_{R47V,D48N,M258C,G259Q}$ revealed that Arg24 interacts strongly with Gln262 (see Figures 4B4, 5B4, and 6B4). Moreover, in the simulations on PTP1B$_{R47V,D48N,M258C,G259Q}$ complexed with *p*-NPP or with bound phosphate, Arg24 also interacts with Gln259 (see Figure 7A1,B1). In PTPα, the arginine is a proline, which is not a potential hydrogen bond partner for Gln262 and hence would not affect the mobility of Gln262. To elucidate the effect of this change, we have additionally performed simulations on PTPα complexed with *p*-NPP and on the cysteinyl-phosphate intermediate. As described above, we have monitored the distances along the trajectories and calculated the probability distribution of these distances. The distributions are displayed in Figure 9 for the Michaelis−Menten complex (left panel, A1−A4) and for the cysteinyl-phosphate intermediate (right panel, B1−B4). The probability distributions correspond to the distances Gln259−Gln262 (Figure 9A1,B1), Gln259−Arg254 (Figure 9A2,B2), Gln262−Arg254 (Figure 9A3,B3), and Gln262−Cys215 (Figure 9A4,B4). The overall picture is very similar to that of the simulations on PTP1B$_{R47V,D48N,M258C,G259Q}$. The probability distribution of the distances (and with that respect the interaction energy) between Gln259 and Gln262 is similar for the Michaelis−Menten complex of PTPα (Figure 9A1) and PTP1B$_{R47V,D48N,M258C,G259Q}$ (Figure 7A3). In both cases, a bimodal distribution is found, which is more pronounced for PTPα (Figure 9A1). The results for the cysteinyl-phosphate intermediate (Figures 9B1 and 7B3) show the same features with a maximum population of distances around 4−5 Å. The maximum of the probability distribution of distances between Gln259 and Arg254 are shifted to shorter distances in PTPα (Figure 9A2) when compared with the one for PTP1B$_{R47V,D48N,M258C,G259Q}$ (Figures 7A2). The distributions for the cysteinyl-phosphate intermediate of PTP1B$_{R47V,D48N,M258C,G259Q}$ (Figures 7B2) and PTPα (Figure 9B2) are similar with relatively high population at short distances. The recorded Gln262−Cys215 distances are similar in the simulations on the Michaelis−Menten complex of PTP1B$_{R47V,D48N,M258C,G259Q}$ (Figure 6A1) and PTPα (Figure 9A4). In both systems, steric hindrance does not allow Gln262 to swing into the binding pocket, and consequently, mainly distances above 6−7Å are observed. The distribution of distances for the cysteinyl-phosphate intermediate of PTPα (Figure 9B4) is broader than that observed for PTP1B$_{R47V,D48N,M258C,G259Q}$ (Figure 6B1). The former distribution also has a population of Gln262 conformations at larger distances. The most significant difference is the interaction between Gln262 and Arg254. Here, clear differences can be seen in both cases (i.e., Michaelis−Menten complex and the cysteinyl-phosphate intermediate). In the Michaelis−Menten

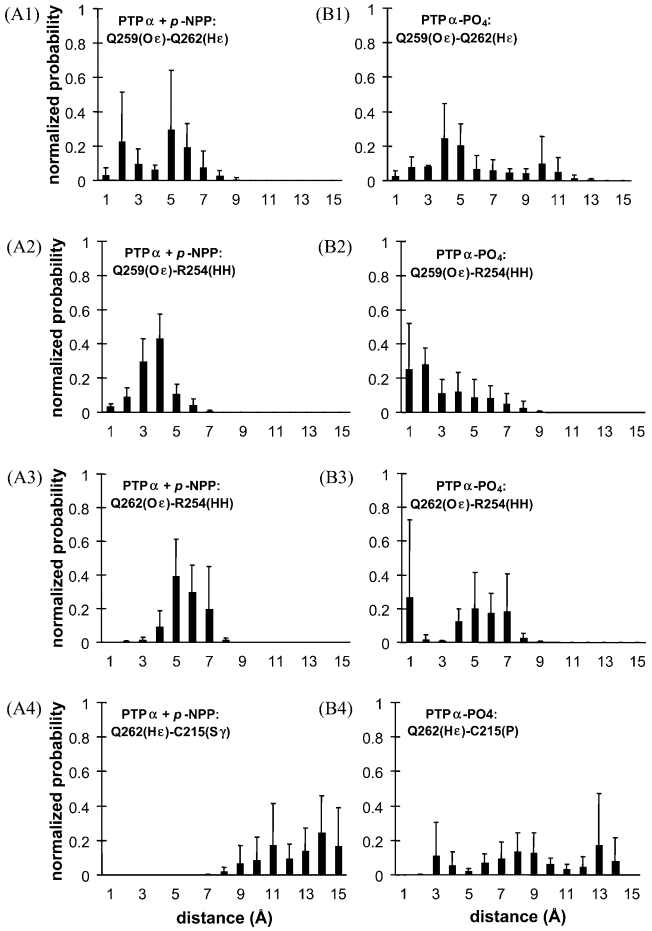

FIGURE 9: Normalized probability functions of distances between selected residues, which are calculated from the time evolution of the distances (data not shown). Distances shown in panels A and B are extracted from the simulations of the model structure of PTPα with bound substrate *p*-NPP and with covalently bound phosphate, respectively. The distances monitored in the PTPα + *p*-NPP simulations are (A1) Q259(Oε)−Q262(Hε), (A2) Q259(Oε)−R254-(HH), (A3) Q262(Oε)−R254(HH), and (A4) Q262(Hε)−C215(Sγ). The corresponding distances extracted from the PTPα−PO_4 simulations are shown on the right and labeled B1−B4. See caption for Figure 5 for definition of the histogram.

complex, the probability distribution of distances is broader in $PTP1B_{R47V,D48N,M258C,G259Q}$ (Figure 6A3) than in PTPα (Figure 9A3). The latter is more populated around 5 Å. In the cysteinyl-phosphate intermediate of $PTP1B_{R47V,D48N,M258C,G259Q}$, only distances above 5−6 Å are observed (Figure 6B3), whereas in PTPα a relatively high population at short distances are found (Figure 9B3). Clearly the bimodal distribution is significantly different from the results of the mutant structure of PTP1B.

Water Molecule Participating in the Second Step of Hydrolysis. In the second step of catalysis, involving hydrolysis of the phosphoenzyme, a water molecule acts as a nucleophile. As mentioned above, the reaction requires that the hydrolytic water molecule is positioned correctly relative to the covalently bound phosphate moiety in the active site bridging the side chain of Gln262 and the Cys215 with a phophorus covalently attached. A hydrogen bond interaction from the side chain of Gln262 restricts the motion of the water molecule. Hence a prerequisite for catalysis is the positioning of a water molecule in close vicinity to both of these side chains. To quantify the influence of the side chain

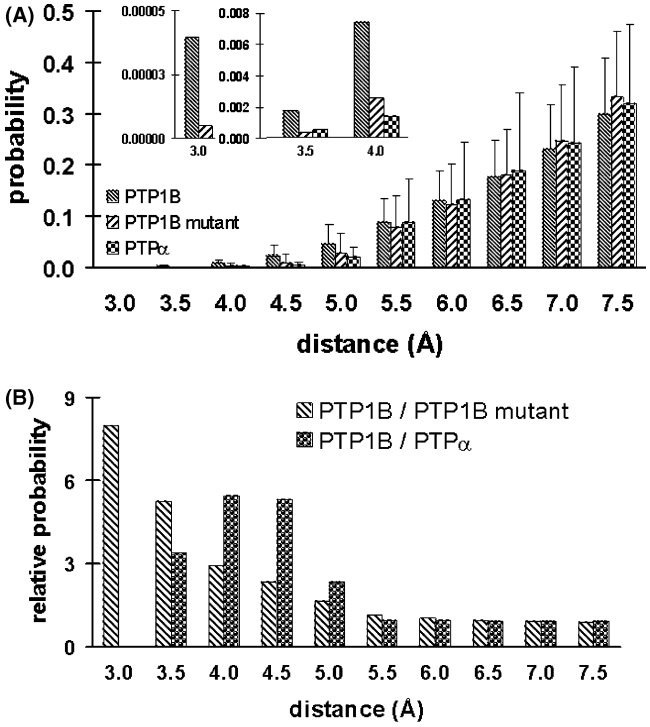

FIGURE 10: The probability density of water molecules within a distance of both Gln262 and Cys215 are shown vs distance. The distance from a water molecule to Gln262 has been determined as the distance between the oxygen of the water to one of the amide atoms of the side chain of Gln262. Similarly the distance from a water molecule to the phosphorylated Cys215 has been determined as the distance between the water oxygen and one of the oxygens of phosphate of the phosphorylated Cys215. Hence the probability, for example, at the distance equal to 3 Å corresponds to the probability of finding a molecule within a distance of 3 Å from both Gln262 and Cys215. In panel A, the probability densities of water molecules are shown, while in panel B, the relative probability densities are shown. Note that within the time frame of the simulations on PTPα no water molecules were found within 3 Å resulting in a ratio PTP1B/PTPα equals infinity (not shown in the graph).

in position 259 on the potential catalytic water molecules, we have measured the probability of water molecules being at a certain distance from both of the side chains 215 and 262 in the MD simulations on the three different cysteine-phosphor complexes. In Figure 10A, the results are shown in terms of probabilities as a function of distance for PTP1B, $PTP1B_{R47V,D48N,M258C,G259Q}$, and PTPα. For large distances, as expected, the probability in each of the simulations approaches the same value. However, for small distances, large differences are observed. These differences are substantiated in Figure 10B, where the relative probabilities have been plotted as a function of distances from both side chains, 215 and 262. Hence, the probability of finding a water molecule in a distance less than 3 Å is approximately 8 times larger in PTP1B than in $PTP1B_{R47V,D48N,M258C,G259Q}$. For large distances, the relative probability approaches unity indicating that the occurrence of water molecules at a particular distance is the same in PTP1B, $PTP1B_{R47V,D48N,M258C,G259Q}$, and PTPα. This analysis suggests that the presence of a glutamine in position 259 interferes with Gln262 resulting in a reduced propensity for correct positioning of the catalytic water molecule. This finding is reflected in the experimental observation that k_{cat} is significantly lower for $PTP1B_{R47V,D48N,M258C,G259Q}$ and PTPα than for PTP1B with

p-NPP as substrate (*31*). Hence, k_{cat} for PTPα is decreased due to the impact of Gln259 on (i) Gln262 conformational freedom, (ii) substrate binding, and (iii) water positioning.

SUMMARY

Experimental work points to a complex picture regarding the function of residue 259 in substrate recognition and hydrolysis. Therefore, to evaluate the influence of residue 259 on the catalytically important residue Gln262, we have performed a set of molecular modeling experiments: adiabatic conformational search and molecular dynamics simulations on the catalytic domain crystal structures of PTP1B, a model of the active form of $PTP1B_{R47V,D48N,M258C,G259Q}$, and a model of the active form of PTPα. The latter two enzymes are representative for PTPs with bulky residues in position 259. For each enzyme two cases are modeled: the Michaelis−Menten complex with the substrate analogue *p*-nitrophenyl phosphate bound to the active site and the cysteinyl-phosphate intermediate. The simulations are analyzed to elucidate the conformational space explored by Gln262 along the trajectories and to identify key interactions between Gln262 and residues residing in the vicinity of Gln262 that might affect the dynamics of Gln262. First an adiabatic conformational search was conducted. The qualitative conclusion from this approach was that a bulky side chain in position 259 restricts the conformational space of Gln262 in the Michaelis−Menten complex as well as in the cysteinyl-phosphate intermediate. Hence, the side chain of Gln262 in PTP1B adopts a wide spectrum of low-energy conformations, which in both the mutant $PTP1B_{R47V,D48N,M258C,G259Q}$ and PTPα is considerably reduced. The results from this approach reflect the experimental observations: the presence of a bulky side chain in position 259 results in increased K_m and decreased k_{cat}. To further elucidate the mobility of Gln262 and potential interactions to other side chains, we have performed MD simulations. The analysis of the trajectories from the Michaelis−Menten complex of PTB1B revealed that the side chain of Gln262 is tightly engaged in a hydrogen bond interaction to the carbonyl oxygen of Gly259. In the mutant $PTP1B_{R47V,D48N,M258C,G259Q}$, the side chain of Gln262 mainly interacts with the side chain of Arg24 and less frequently with the main chain carbonyl oxygen and the side chain of Gln259. The latter side chain shows a very persistent contact to the side chain of Arg24. For the cysteinyl-phosphate intermediate, Gln262 in PTP1B oscillates between Cys215 and Arg24. In the corresponding mutant complex, Gln262 shows low probability of approaching Cys215. Instead Gln262 interacts primarily with Arg24. Interestingly, the side chain of Gln259 in this complex interacts tightly with Arg254. The same set of modeling experiments was applied to PTPα, and apart from the Arg24−Gln259 interactions, the results resembled those discovered for the mutant $PTP1B_{R47V,D48N,M258C,G259Q}$. Finally, the densities of water molecules in the vicinity of both Gln262 and Cys215 were analyzed in the models of the cysteinyl-phosphate intermediates for the three enzymes. The probability of finding a water molecule positioned in close vicinity of both Gln262 and Cys215 is much larger in PTP1B than in $PTP1B_{R47V,D48N,M258C,G259Q}$ and PTPα. Hence, the probability of finding a water molecule within 3 Å of the two side chains is 8 times larger for PTP1B than for $PTP1B_{R47V,D48N,M258C,G259Q}$. The corresponding probability of finding a water molecule within 3.5 Å is 6 times larger for PTP1B than for $PTP1B_{R47V,D48N,M258C,G259Q}$ and 3.5 times larger for PTP1B than for PTPα.

A glutamine at position 259 is not very frequently encountered in PTPs and is only present in PTPα and PTPϵ. However, in seven human PTPs known today (PTPro, PTPpsi, PTPPCP2, PTPFMI, PTPρ, PTPμ, PTPκ), an asparagine is at position 259 (*29*), which due to their common amide in the side chains may have the same potential to form hydrogen bonds with Gln262. This points to the notion that the interaction between the gatekeeper in position 259 and Gln262 is an important player in the regulation of the activity for a considerable number of PTPs.

The overall conclusion of the present study is that the results obtained from modeling experiments match the experimental findings but also give insight to dynamics and the probability densities of atomic interactions at the molecular level that cannot be elucidated by conventional experiments such as X-ray diffraction.

ACKNOWLEDGMENT

Simulations were performed at the Danish Center for Scientific Computing at the University of Southern Denmark and at Novo Nordisk A/S.

REFERENCES

1. Fisher, E. H., Charbonneau, H., and Tonks, N. K. (1991) Protein tyrosine phosphatases, *Science 253*, 401−406.
2. Pawson, T., and Scott, J. D. (1995) Signaling through scaffold, anchoring, and adaptor proteins, *Science 278*, 2075−2080.
3. Hunter, T. (1995) Protein kinases and phosphatases: the yin and yang of protein phosphorylation and signaling, *Cell 80*, 225−236.
4. Zhang, Z. Y. (2002) Protein tyrosine phosphatases: structure and function, substrate specificity, and inhibitor development, *Annu. Rev. Pharmacol. Toxicol. 42*, 209−234.
5. Ostman, A., and Heldin, C. H. (2001) Involvement of platelet-derived growth factor in disease: development of specific antagonists, *Adv. Cancer Res. 80*, 1−38.
6. Robertson, S. C., Tynan, J. A., and Donoghue, D. J. (2000) RTK mutations and human syndromes when good receptors turn bad, *Trends Genet. 16*, 265−271.
7. Hunter, T. (1997) Oncoprotein networks, *Cell 88*, 333−346.
8. Ng, J. H., and Ilag, L. L. (2002) Functional proteomics: separating the substance from the hype, *Drug Discovery Today 7*, 504−505.
9. Johnson, T. O., Ermolieff, J., and Jirousek, M. R. (2002) Protein tyrosine phosphatase 1B inhibitors for diabetes, *Nat. Rev. Drug Discovery 1*, 696−709.
10. Liu, G., and Trevillyan, J. M. (2002) Protein tyrosine phosphatase 1B as a target for the treatment of impaired glucose tolerance and type II diabetes, *Curr. Opin. Invest. Drugs 3*, 1608−1616.
11. Zhang, Z. Y. (2001) Protein tyrosine phosphatases: prospects for therapeutics, *Curr. Opin. Chem. Biol. 5*, 416−423.
12. Dadke, S., and Chernoff, J. (2003) Protein-tyrosine phosphatase 1B as a potential drug target for obesity, *Curr. Drug Targets: Immune Endocr. Metab. Disord. 3*, 299−304.
13. Boute, N., Boubekeur, S., Lacasa, D., and Issad, T. (2003) Dynamics of the interaction between the insulin receptor and protein tyrosine-phosphatase 1B in living cells, *EMBO Rep. 4*, 313−319.
14. Haj, F. G., Verveer, P. J., Squire, A., Neel, B. G., and Bastiaens, P. I. (2002) Imaging sites of receptor dephosphorylation by PTP1B on the surface of the endoplasmic reticulum, *Science 295*, 1708−1711.
15. Ukkola, O., and Santaniemi, M. (2002) Protein tyrosine phosphatase 1B: a new target for the treatment of obesity and associated co-morbidities, *J. Intern. Med. 251*, 467−475.
16. Goldstein, B. J. (2001) Protein-tyrosine phosphatase 1B (PTP1B): a novel therapeutic target for type 2 diabetes mellitus, obesity and related states of insulin resistance, *Curr. Drug Targets: Immune Endocr. Metab. Disord. 1*, 265−276.

17. Tonks, N., and Neel, B. G. (2001) Combinatorial control of the specificity of protein tyrosine phosphatases, *Curr. Opin. Cell Biol. 13*, 182−195.
18. Ostman, A., and Bohmer, F. D. (2001) Regulation of receptor tyrosine kinase signaling by protein tyrosine phosphatases, *Trends Cell Biol. 11*, 258−266.
19. Zhang, Z. Y. (1998) Protein-tyrosine phosphatases: biological function, structural characteristics, and mechanism of catalysis, *Crit. Rev. Biochem. Mol. Biol. 33*, 1−52.
20. Denu, J. M., and Dixon, J. E. (1998) Protein tyrosine phosphatases: mechanisms of catalysis and regulation, *Curr. Opin. Chem. Biol. 2*, 633−641.
21. Barford, D. (1995) Protein phosphatases, *Curr. Opin. Struct. Biol. 5*, 728−734.
22. Barford, D., Das, A. K., and Egloff, M. P. (1998) The structure and mechanism of protein phosphatases: insights into catalysis and regulation, *Annu. Rev. Biophys. Biomol. Struct. 27*, 133−164.
23. Zhang, Z. Y., Wang, Y., Wu, L., Fauman, E. B., Stuckey, J. A., Schubert, H. L., Saper, M. A., and Dixon, J. E. (1994) The Cys-(X)5Arg catalytic motif in phosphoester hydrolysis, *Biochemistry 33*, 15266−15270.
24. Fauman, E. B., and Saper, M. A. (1996) Structure and function of the protein tyrosine phosphatases. *Trends Biochem. Sci. 21*, 413−417.
25. Barford, D., Flint, A. J., and Tonks, N. K. (1994) Crystal structure of human protein tyrosine phosphatase 1B. *Science 263*, 1397−1404.
26. Peters, G. H., Frimurer, T. M., and Olsen, O. H. (1998) Electrostatic evaluation of the signature motif (H/V)CX_5R(S/T) in protein-tyrosine phosphatases. *Biochemistry 37*, 5383−5393.
27. Pot, D. A., and Dixon, J. E. (1992) A thousand and two protein tyrosine phosphatases, *Biochim. Biophys. Acta 1136*, 35−43.
28. Streuli, K., Krueger, N. X., Thai, T., Tang, M., and Saito, H. (1990) Distinct functional roles of the two intracellular phosphatase like domains of the receptor-linked protein tyrosine phosphatases LCA and LAR, *EMBO J. 9*, 2399−2407.
29. Andersen, J. N., Mortensen, O. H., Peters, G. H., Drake, P. G., Iversen, L. F., Olsen, O. H., Andersen, H. S., Tonks, N. K., and Møller, N. P. H. (2001) Structural and Evolutionary Relationships among Protein Tyrosine Phosphatase Domains, *Mol. Cell. Biol. 21*, 7117−7136.
30. Iversen, L. F., Andersen, H. S., Branner, S., Mortensen, S. B., Peters, G. H., Norris, K., Olsen, O. H., Jeppesen, C. B., Lundt, B. F., Ripka, W., Møller, K. B., and Møller, N. P. H. (2000) Structure-based design of a low molecular weight, nonphosphorus, nonpeptide, and highly selective inhibitor of protein-tyrosine phosphatase 1B, *J. Biol. Chem. 275*, 10300−10307.
31. Peters, G. H., Iversen, L. F., Branner, S., Andersen, H. S., Mortensen, S. B., Olsen, O. H., Møller, K. B., and Møller, N. P. H. (2000) Residue 259 is a key determinant of substrate specificity of protein-tyrosine phosphatases 1B and alpha, *J. Biol. Chem. 275*, 18201−18209.
32. Salmeen, A., Andersen, J. N., Myers, M. P., Tonks, N. K., and Barford, D. (2000) Molecular basis for the dephosphorylation of the activation segment of the insulin receptor by protein tyrosine phosphatase 1B, *Mol. Cell 6*, 1401−1412.
33. Puius, Y. A., Zhao, Y., Sullivan, M., Lawrence, D. S., Almo, S. C., and Zhang, Z. Y. (1997) Identification of a second aryl phosphate-binding site in protein-tyrosine phosphatase 1B: a paradigm for inhibitor design, *Proc. Natl. Acad. Sci. U.S.A. 94*, 13420−13425.
34. Pannifer, A. D., Flint, A. J., Tonks, N. K., and Barford, D. (1998) Visualization of the cysteinyl-phosphate intermediate of a protein-tyrosine phosphatase by X-ray crystallography. *J. Biol. Chem. 273*, 10454−10462.
35. Jia, Z., Barford, D., Flint, A. J. and Tonks, N. K. (1995) Structural basis for phosphotyrosine peptide recognition by protein tyrosine phosphatase 1B, *Science 268*, 1754−1758.
36. Bilwes, A. M., Den Hertog, J., Hunter, T., and Noel, J. P. (1996) Structural basis for inhibition of receptor protein-tyrosine phosphatase- alpha by dimerization, *Nature 382*, 555−558.
37. Bernstein, F. C., Koetzle, T. F., Williams, G. J. B., Meyer, E. F., Brice, M. D., Rogers, J. R., Kennard, O., Shimanouchi, T., and Tasumi, M. (1977) The Protein Data Bank: a computer-based archival file for macromolecular structure, *J. Mol. Biol. 112*, 535−542.
38. Brooks, B. R., Bruccoleri, R. E., Olafson, B. D., States, D. J., Swaminathan, S., and Karplus, M. (1983) CHARMM: a program for macromolecular energy minimization, and dynamics calculation. *J. Comput. Chem. 4*, 187−217.
39. Jørgensen, W. L., Chandrasekhar, J., Medura, J. D., Impey, R. W., and Klein, M. L. (1983) Comparison of simple potential functions for simulation liquid water, *J. Chem. Phys. 79*, 926−935.
40. Van Gunsteren, W. F., Beutler, T. C., Fraternali, F., King, P. M., Mark, A. E., and Smith, P. E. (1994) Computation of free energy in practice: Choice of approximations and accuracy limiting factors, in *Computer Simulations in Biological Systems* (van Gunsteren, W. F., Weiner, P. K., and Wilkinson, A. J., Eds), Escon, Leiden, The Netherlands.
41. Peters, G. H., Frimurer, T. M., Andersen, J. N., and Olsen, O. H. (1999) Molecular dynamics simulations of protein-tyrosine phosphatase 1B. I. ligand-induced changes in the protein motions, *Biophys. J. 77*, 505−515.
42. Peters, G. H., Frimurer, T. M., Andersen, J. N., and Olsen, O. H. (2000) Molecular dynamics simulations of protein-tyrosine phosphatase 1B. II. substrate-enzyme interactions and dynamics, *Biophys. J. 78*, 2191−2200.
43. Zhao, Y., Wu, L., Noh, S. J., Guan, K.-L., and Zhang, Z.-Y. (1998) Altering the nucleophile specificity of a protein-tyrosine phosphatase-catalyzed reaction. Probing the function of the invariant glutamine residues, *J. Biol. Chem. 273*, 5484−5492.
44. Tonks, N. K. (2003) PTP1B: from the sidelines to the front lines! *FEBS Lett. 546*, 140−148.
45. Xie, L., Zhang, Y. L., and Zhang, Z. Y. (2002) Design and characterization of an improved protein tyrosine phosphatase substrate-trapping mutant, *Biochemistry 41*, 4032−4039.
46. Iversen, L. F., Andersen, H. S., Møller, K. B., Olsen, O. H., Peters, G. H., Branner, S., Mortensen, S. M., Hansen, T. K., Lau, J., Ge, Y., Holsworth, D. D., Newman, M. J., and Møller, N. P. H. (2001) Steric hindrance as a basis for structure-based design of selective inhibitors of protein-tyrosine phosphatases, *Biochemistry 40*, 14812−14820.
47. Peters, G. H., Branner, S., Møller, K. B., Andersen, J. N., and Møller, N. P. H. (2003) Enzyme kinetic characterization of protein tyrosine phosphatases, *Biochimie 85*, 527−534.
48. Zabolotny, J. M., Bence-Hanulec, K. K., Stricker-Krongrad, A., Haj, F., Wang. Y., Minokoshi, Y., Kim, Y. B., Elmquist, J. K., Tartaglia, L. A., Kahn B. B., and Neel, B. G. (2002) PTP1B regulates leptin signal transduction in vivo, *Dev. Cell 2*, 489−495.
49. Pallen, C. J. (2003) Protein tyrosine phosphatase alpha (PTPalpha): a Src family kinase activator and mediator of multiple biological effects, *Curr. Top. Med. Chem. 3*, 821−835.
50. Skelton, M. R., Ponniah, S., Wang, D. Z.-M., Doetschman, T., Vorhees, C. V., and Pallen, C. J. (2003) Protein tyrosine phosphatase alpha (PTP alpha) knockout mice show deficits in Morris water maze learning, decreased locomotor activity, and decreases in anxiety, *Brain Res. 984*, 1−10.
51. Tobin, J. F., and Tam, S. (2002) Recent advances in the development of small molecule inhibitors of PTP1B for the treatment of insulin resistance and type 2 diabetes, *Curr. Opin. Drug Discov. Dev. 5*, 500−512.
52. Taylor, S. D. (2003) Inhibitors of protein tyrosine phosphatase 1B (PTP1B), *Curr. Top. Med. Chem. 3*, 759−782.

BI0498757